

# Extremes in temperature and precipitation around the Mediterranean basin in an ensemble of future climate scenario simulations

K. Goubanova\*, L. Li

*Laboratoire de Météorologie Dynamique, LMD/IPSL/CNRS/UPMC, Paris, France*

Available online 29 December 2006

## Abstract

A variable-grid atmospheric general circulation model, the LMDZ, with a local zoom over the Mediterranean is used to investigate potential future changes in climate extremes around the Mediterranean basin. Changes in extremes of annual minimum and maximum temperature, winter and summer 24-h maximum precipitation are discussed under the IPCC-A2 emission scenario. Three time slices of 30 years are chosen to represent respectively the end of the 20th century, the middle and the end of the 21st century. The boundary conditions were taken from the outputs of three global coupled climate models: from the Institut Pierre-Simon Laplace (IPSL), Centre National de Recherches Météorologiques (CNRM) and Geophysical Fluid Dynamics Laboratory (GFDL). These three global scenarios were used to estimate uncertainties associated with climate models. Extreme events are expressed in terms of return values, estimated from a Generalized Extreme Value distribution fitted to annual or seasonal extremes. The changes in distribution of extremes are analyzed to elucidate the nature of the changes in extremes.

Magnitudes and main spatial patterns of the changes in extremes show a quite good consistency among three global scenarios. Comparison between changes in the middle and at the end of the 21st century does not reveal any remarkable discontinuity in future climate evolution. The maximum of warming occurs over Northeastern Europe for annual minimum temperature and over South Europe for annual maximum temperature. Averaged over the region, increase in cold extremes exceeds that in warm extremes. Changes in temperature extremes are mostly associated with shift of whole distribution (location parameter change) and in addition, for cold extremes, with changes in interannual variability, measured by the scale parameter. Mean precipitation changes are characterized by strong reduction belt over the Mediterranean and South Europe in winter, spring and summer. Precipitation extremes increase in all seasons except summer. These changes are predominantly associated with changes in the scale, but also with changes in the position and shape of the distribution. In general terms, it is suggested that the Mediterranean basin will experience a warmer climate with less total precipitation but more intense precipitation events.

© 2006 Elsevier B.V. All rights reserved.

*Keywords:* climate change; climate extremes; Mediterranean basin; Generalized Extreme Value distribution

## 1. Introduction

The Mediterranean basin is particularly vulnerable to present and future climate variability and climate

change. Due to its unique geographic location, this region is a transition zone between the very hot and dry African climate regime in the South and the mild and humid European climate in the North, having hence large climate variations. It is characterized by winter rains and summer droughts. The strong difference between the wet winter and the dry summer is caused by the seasonal

\* Corresponding author.

*E-mail address:* [goubanova@lmd.jussieu.fr](mailto:goubanova@lmd.jussieu.fr) (K. Goubanova).

alternation of the dominance of cyclonic storms in winter and subtropical high pressure cells over adjacent ocean causing dry conditions in summer.

There is a general agreement that impacts of climate changes on society and ecosystem are likely to result rather from changes in climate variability and extremes than from changes in mean climate (Kunkel et al., 1999). The recent extreme events over the Mediterranean basin (flooding in Algeria in November 2001; European summer heat wave in 2003; 2004 winter cold wave in Turkey; heavy snow in Balkan in 2005) pose us the question whether the climate in this region is becoming more variable and more extreme. Along last decades, the climate extreme changes registered in the Mediterranean basin consist of an increase in heavy precipitations and a raise of extreme temperatures. Frich et al. (2002) reported a relative increase in the duration of heat waves and a relative decrease in the number of frost days during the second half of the 20th century over most of the Mediterranean basin. Klein Tank and Können (2003) found that pronounced warming between 1976 and 1999 is primarily associated with increase in warm extremes rather than with a decrease in cold extremes and that in wet areas the changes in extreme precipitation are disproportionately larger than relative changes in the total amount. Alpert et al. (2002) analyzed Mediterranean station records for the period 1951–1995 and showed an increase of daily rainfall together with a decrease in the mean values. A number of previous studies of future climate (Sánchez et al., 2004; Palutikof and Holt, 2004, Giorgi et al., 2004; Gao et al., 2006) revealed significant changes in extremes over the Mediterranean.

Global ocean-atmosphere coupled models are certainly the best tool that we have to make future climate scenario projections. Due to their coarse spatial resolution, they can be hardly used in impact-oriented studies for which a downscaling procedure is necessary. A widely used approach to do it is to use a high-resolution limited-area model nested into the global models. This approach allows implementation of much detailed physical parameterizations in regional climate models (RCM) to ensure a better simulation of local weather and climate events. Another existing approach is based on the use of variable-grid (zoomed) general circulation models (GCM) with closer resolution for the study region. This provides an improved downscaling of information from large scale to regional scale, but the maximum resolution is currently strongly limited, due to either computing capacity or physical parameterizations implemented in such GCMs.

Most of the recent research programmes on climate variability and change over Europe (STARDEX, <http://www.cru.uea.ac.uk/projects/stardex/>; MICE, <http://www.cru.uea.ac.uk/projects/mice/>;

PRUDENCE, Christensen et al., 2002) and related studies include only partially the Mediterranean basin as the southmost part of their considered domain. Due to the marginal effects, simulated climates over the Mediterranean basin are often biased by the prescription of the boundary conditions. This decreases largely the validity of such studies on the Mediterranean climate.

In this paper we estimate future changes of temperature and precipitation in the Mediterranean basin by using a variable resolution GCM with a stretched grid. The main objective of our study is to document simulated changes of extremes around the Mediterranean basin for both temperature and precipitation. Extremes are expressed in terms of return values derived from a Generalized Extreme Value (GEV) distribution. We analyze changes in the distribution parameters to understand the nature of changes in extremes and the changes in variability of the climate variables. The middle and the end of the 21st century were analyzed to determine whether the response of climate variables to global warming is monotone during the 21st century or the primary warming can further induce abrupt changes. We address the issue of uncertainties by performing three scenarios from three different global coupled GCMs.

Section 2 presents the used model and the performed climate change experiments. Section 3 describes the methodology for estimating extreme values and significance of their changes in future climate. The temperature and precipitation extreme changes are examined in Section 4. This section also discusses the distribution parameters changes. Conclusions are summarized in Section 5.

## 2. Model and simulations

The model used to evaluate the Mediterranean climate change behaviours is the LMDZ-Mediterranean, a global variable-grid atmospheric GCM with zoom over the Mediterranean Sea. The effective resolution of the model is about  $150 \times 150 \text{ km}^2$ . In this study, the version 4.0 of LMDZ is used. It is derived from the standard version described in Sadourny and Laval (1984). A brief presentation of the current physical parameterization is in Li (1999). The convection schema has been changed, since then, to that developed by Emanuel (1991).

The LMDZ-Mediterranean employs, as lower boundary conditions and driving forcing, the sea-surface temperature (SST), sea-ice extension and greenhouse-gas concentrations to make regionally oriented simulations. Unlike the nesting approach that needs to incorporate a regional model into a large-scale global model, our

Table 1

List of simulations conducted with LMDZ-Mediterranean for different periods and with different boundary conditions

Simulation	Period	Boundary conditions
exp00	1970/1999	Observed SST and sea-ice
exp101	2030/2059	A2 scenario from IPSL
exp102		CNRM
exp103		GFDL
exp03	2070/2099	A2 scenario from IPSL
exp04		CNRM
exp05		GFDL

approach with a variable-grid GCM is operating in a standalone manner. For the control simulation (referred to as LMDZ/CTRL, hereafter) dedicated to reproduce the current climate, the observed climatological conditions from 1979 to 1999 are used. For future climate evolution, we use outputs from three global coupled climate models run in the Institut Pierre-Simon Laplace, IPSL (Dufresne et al., 2002), Centre National de Recherches Météorologiques, CNRM (Gibelin and Déqué, 2003) and Geophysical Fluid Dynamics Laboratory, GFDL (Delworth et al., 2002). Simulations with outputs of these global models will be referred to as LMDZ/IPSL, LMDZ/CNRM and LMDZ/GFDL respectively. All of them give the future climate projection under the hypothesis of A2 emission scenario (IPCC, 2001). The three global models are state-of-the-art ocean-atmosphere coupled models. Their dispersion comes mainly from differences in their physics and the parameterization of physical processes. This will permit us to assess uncertainty related to the physics of global climate models. This uncertainty is currently believed to represent half of the total uncertainty in future projection of global climate, the other half being related to the emission scenarios of greenhouse gases (IPCC, 2001). Furthermore we use here a regionally oriented model to refine the climate projection at a regional scale, this may introduce another uncertainty, but we cannot evaluate it since only one model is used.

To make the results from the three global scenarios easily comparable, we have adopted the approach of “anomalies” in constructing the boundary conditions to be used in LMDZ-Mediterranean, i.e., we calculated firstly the differences of forcing variables (SST and sea ice extension) between the future state and the present-day state of the global models. We then added such anomalies to observed values of current climate. In such a manner, we need to produce only one control simulation for all scenarios. We select two future periods for our study, one is the average conditions from 2070 to 2099 (the middle is the yr 2085) which is intended to represent the end of the 21st century, another is from 2030 to 2059 (the middle is

the yr 2045) which is to represent the middle of the 21st century. A list of LMDZ experiments analyzed in this work is shown in Table 1.

### 3. Methodology

One commonly used method to describe extreme climate events is to use some high quantiles for the annual or seasonal empirical distribution of examined climate variable. But high quantiles are much affected by sampling uncertainties. Furthermore it is usually required to estimate the probability of events that are more extreme than any that have been observed. Using a theoretic distribution function to fit a sample of extremes is therefore a more appropriate way to describe rare events. In our study we apply the Generalized Extreme Value (GEV) distribution, as described in Zwiers and Kharin (1998) and Kharin and Zwiers (2000).

The GEV distribution is very largely used in meteorology and hydrology to describe extreme values. The theoretical background for this approach is the extremal limit theorem (Fisher and Tippett, 1928) saying that the maximum or minimum of a sample asymptotically follows a GEV distribution that combines the three possible extreme value distributions predicted by large sample theory, i.e., the Gumbel, Fréchet and Weibull distributions (see Coles, 2001 for a more detailed description on the related statistical theory). The cumulative distribution function of the GEV is given by:

$$F(x) = \begin{cases} \exp(-[1-k(x-\xi)/\alpha]^{1/k}), & k < 0, x > \xi + \alpha/k, \\ \exp(-\exp[-(x-\xi)/\alpha]), & k = 0, \\ \exp(-[1-k(x-\xi)/\alpha]^{1/k}), & k > 0, x < \xi + \alpha/k, \end{cases}$$

where  $\xi$  is a location parameter representing the overall position of the distribution,  $\alpha$  is a scale parameter that

Table 2

Percentage of grid points where the null hypothesis (the samples of extremes in control run are drawn from the GEV distribution) is rejected at the 5% significance level. Results are averaged over the three global scenarios and for all the simulations, control and two future periods

		LMDZ/Control	$\Delta$ 2045	$\Delta$ 2085
Tmax		4.5	8.1	7.9
Tmin		7.9	5.1	7.4
Pre	DJF	19.3	20.1	19.8
	JJA	36.1	41.6	44.0
	MAM	22.7	22.5	24.6
	SON	21.8	22.2	22.6

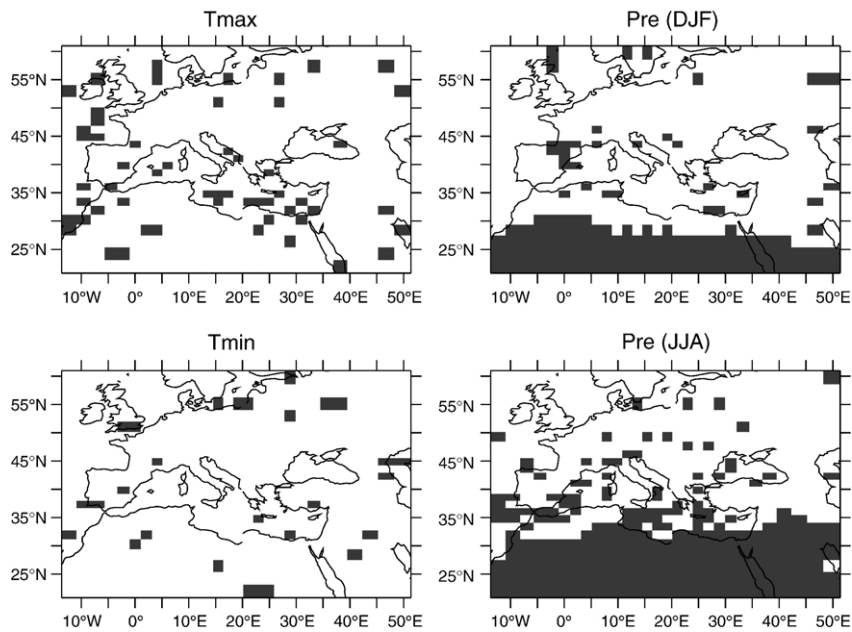


Fig. 1. Kolmogorov–Smirnov test for GEV distribution fitted to samples of extremes in control run. Shading indicates areas where the null hypothesis that the samples originated from GEV distribution is rejected at the 5% significance level.

characterizes the spread of the distribution and  $k$  is the shape parameter determining type of extreme value distribution. The special case of the GEV distribution with  $k=0$  defines the Gumbel distribution, which is a limiting distribution of extremes drawn from many standard distributions, including the normal and exponential distributions. The Weibull distribution ( $k>0$ ) has bounded upper tail. The Fréchet distribution ( $k<0$ ) is heavy-tailed, that is, the upper tail of its probability density function converges to 0 at a slower rate than that of the other two distributions.

There are two most commonly used methods to estimate the distribution parameters: maximum likelihood estimators and  $L$ -moments. Because of their computational simplicity and good performance for

small samples we employed the method of  $L$ -moments (Hosking, 1990, 1992) following the procedure outlined by Zwiers and Kharin (1998). Extremes will be expressed in terms of return values. The return value associated with the desired period  $T$  is given by inverting the fitted GEV distribution:

$$X_T = \begin{cases} \xi + \hat{\alpha}(1 - [-\ln(1-1/T)]\hat{k})/\hat{k}, & \hat{k} \neq 0, \\ \xi - \hat{\alpha} \ln[-\ln(1-1/T)], & \hat{k} = 0. \end{cases}$$

This is the threshold that is expected to be exceeded once every  $T$  years.

To examine the feasibility of the GEV distribution to simulated extremes the standard Kolmogorov–Smirnov test was applied. The idea of this goodness-of-fit test is

Table 3

Percentage of grid points where the changes in return values and in GEV distribution parameters are statistically significant at the 10% significance level. Results are the ensemble average for the three global scenarios

		$\Delta 2045$				$\Delta 2085$			
		rv30	$\xi$	$\alpha$	$k$	rv30	$\xi$	$\alpha$	$k$
Tmax		74.4	92.4	28.4	24.9	94	99.3	31.5	28.2
Tmin		75.4	84	25.2	23.1	99.1	99.7	25.8	30
Pre	DJF	34.8	35.7	32.9	22.3	49.5	56.6	42.6	26
	JJA	31.4	41.3	32.9	24.8	32.4	52.1	34.5	28.1
	MAM	27.4	31.6	25	21.9	31.4	49.7	34.1	28.1
	SON	34	31.7	30	23.8	44	47.4	37.7	25.5

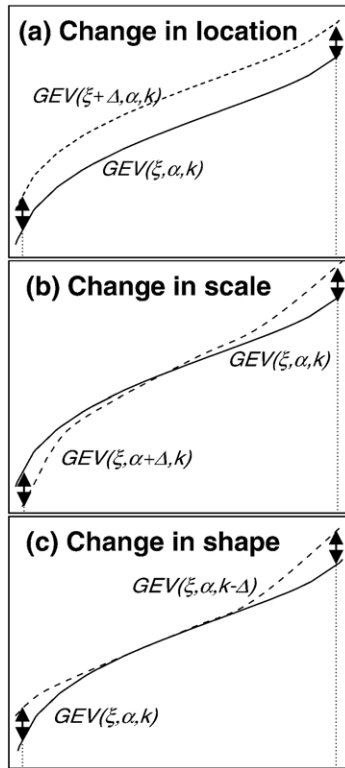


Fig. 2. Schematic diagram representing how changes in parameters of GEV distribution can affect changes in extremes at both ends of the distribution function.

simply to find the maximum difference between empiric and theoretic cumulative distribution functions:

$$D = \max_{-\infty < x < \infty} |F(x) - G_N(x)|,$$

where  $F(x)$  is the fitted distribution function and  $G_N(x)$  the empirical distribution function estimated from the sample. When this maximum exceeds a certain value the null hypothesis that the extremes are drawn from the fitting function is rejected. Since the location, scale, and shape parameters are estimated from the data, this critical value should not be obtained from statistical tables (Durbin, 1976). Consistent estimate of the critical value can be found by the parametric bootstrap procedure (Babu and Rao, 2004). We generated 1000 samples of the same size as modelling series of extremes from each fitted GEV distribution. The 95th quantile of  $\{D_i\}_{i=1:1000}$  derived from resulting family was employed as the critical value for the rejection of the null hypothesis that the simulated sample of extremes descends from the GEV distribution at the 5% significant level. Table 2 shows the percentage of grid points where the null hypothesis that the samples of temperature and precip-

itation extremes in control run are drawn from the GEV distribution is rejected at the 5% significance level. The GEV distribution fits the temperature extremes much better than the precipitation ones. In Fig. 1 the spread of the grid points where the null hypothesis is rejected is shown for annual maximum temperature, annual minimum temperatures and precipitation in winter and summer seasons. In spring and autumn the spread for the precipitation is similar to those in winter. In the case of the temperature the “bad” points are randomly scattered whereas the rejecting of the null hypothesis that the seasonal precipitation extremes originate from the GEV distribution takes place mainly over the area with too small rainfalls (the most of annual maximums are zero, and the assumption of data independence of the extremal limit theorem is not fulfilled). It is worthy to note that this area mainly expands in the future climate in the summer season for all the simulations (not shown).

In the following we will present the changes in the extremes (the difference between the 30-yr return values in each future climate simulation and the control simulation) only for the grid points where the null hypothesis is not rejected. To estimate the statistic significance of these changes, the 90% confidence intervals of the present-climate return values are calculated by the parametric bootstrap procedure where 1000 samples (of size 30) are generated from the fitted GEV distribution. The 5th and 95th percentiles of the set of the return value estimates derived from each generated sample are used as lower and upper 90% confidence bounds for the return value of the initial sample. The changes in  $T$ -yr return values are said to be statistically significant when the future-climate return value does not fall in the 90% confidence intervals of the present-climate return value, that corresponds to a 10% statistical

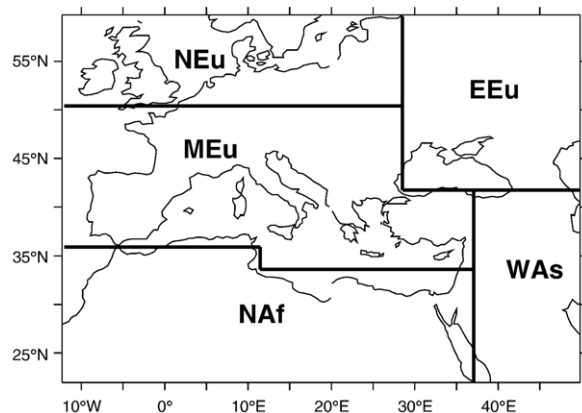


Fig. 3. Definition of subregions.

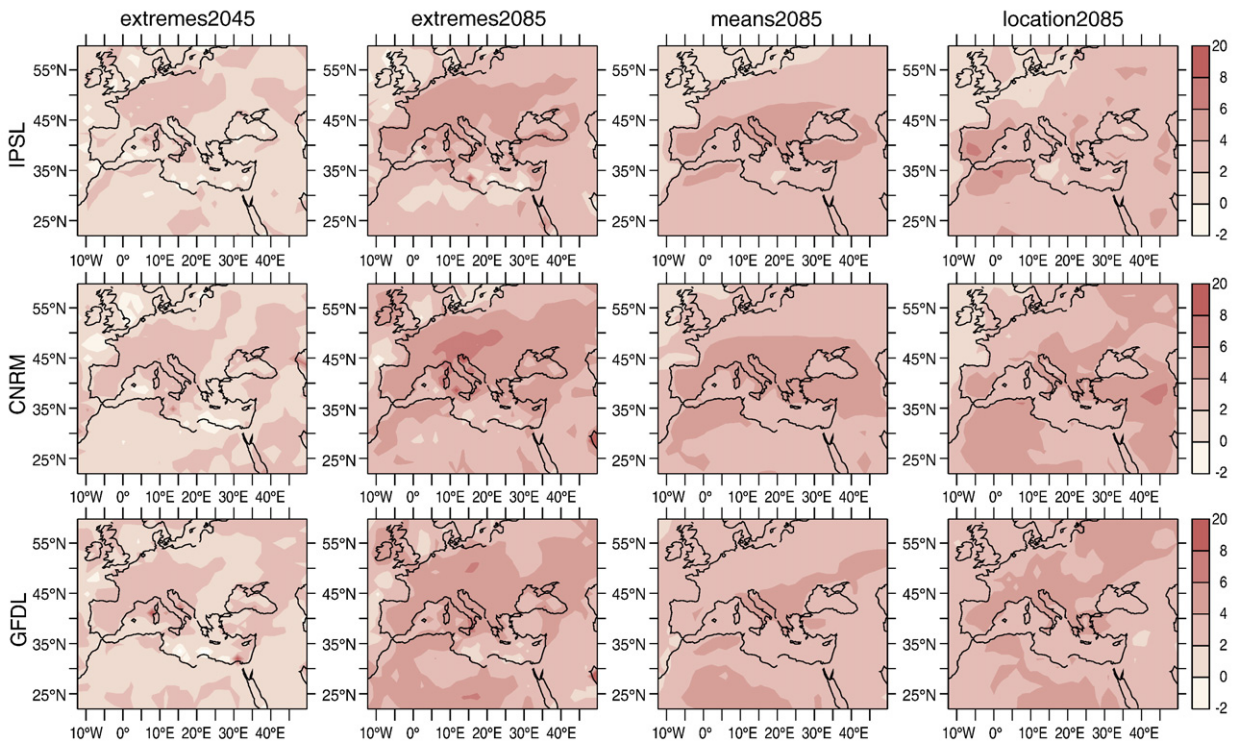


Fig. 4. Future changes of the annual maximum temperature simulated by LMDZ with A2 emission scenario with the three global climate scenarios (IPSL, CNRM and GFDL respectively from top to bottom) relative to 1970/1999: 30-yr return values in 2030/2059, 30-yr return values in 2070/2099, mean values in 2070/2099 and changes in location parameter of the GEV distribution in 2070/2099 respectively from left to right. Units are °C.

significance level. The significance of changes in location, scale and shape parameters is defined in the same manner. Table 3 shows the percentage of area where the difference between the control and future return values is significant in the sense described above. We will again refer to this table in the next section.

We used the GEV distribution parameter changes to better understand the nature of changes in extremes and

estimate the modification of their distribution function. Fig. 2 presents a schematic diagram depicting how changes in parameters modify distribution function, implicating changes in the extreme values. The solid curve represents the GEV cumulative distribution function of a climate variable. Dashed curves indicate the same function when one of the three distribution parameters changed. The corresponding changes in extreme

Table 4

Changes in mean values (°C) and in 30-yr return values (°C) for the annual maximum temperature, and for 5 subregions as indicated in Fig. 2. Under the label LMDZ/Control are given the parameters themselves for the control simulation

		LMDZ/Control	$\Delta 2045$			$\Delta 2085$		
			LMDZ/IPSL	LMDZ/CNRM	LMDZ/GFDL	LMDZ/IPSL	LMDZ/CNRM	LMDZ/GFDL
NEu	Mean	21.6	1.1	1	1.6	2.1	2.5	3.1
	rv30	33.4	1.7	1.1	1.8	2.8	3.8	4
EEu	Mean	27.4	1.5	1.5	1.8	3.2	3.7	3.5
	rv30	37.1	1.5	2.2	2	3.7	4.7	4.2
MEu	Mean	26.9	1.6	1.9	1.7	3.4	4.1	3.4
	rv30	36.8	1.4	2	2	3.7	4.3	4
NAf	Mean	36.6	1.5	1.7	1.6	2.9	3.7	3.6
	rv30	44.6	1.3	1.3	1.6	2.7	3.3	3.9
WAs	Mean	35.4	1.6	2	1.6	3.3	4	3
	rv30	43.6	1.4	2	1.4	2.6	3.9	3.2

Table 5

Spatial correlation coefficients between changes in extreme (30-yr return values) and changes in distribution parameters for the annual maximum temperature. The values significant at the 5% significance level are emphasized in bold

	$\Delta 2045$			$\Delta 2085$		
	LMDZ/ IPSL	LMDZ/ CNRM	LMDZ/ GFDL	LMDZ/ IPSL	LMDZ/ CNRM	LMDZ/ GFDL
$(\Delta r_{p30}, \Delta \xi)$	<b>0.14</b>	<b>0.16</b>	<b>0.15</b>	<b>0.3</b>	<b>0.24</b>	<b>0.34</b>
$(\Delta r_{p30}, \Delta \alpha)$	0.01	0.07	0.08	0.01	-0.03	0.04
$(\Delta r_{p30}, \Delta k)$	0.03	-0.03	0.01	0.01	-0.02	0.05

values at both ends of curves are indicated by the arrows. Changes in location parameter (Fig. 2a) lead to a simple shift of the distribution and suggest change of the mean value. Scale parameter (Fig. 2b), being a measure of variability, “stretches” and “shrinks” the distribution. Shape parameter (Fig. 2c) determines the heaviness of the tail of the distribution.

To display maps of future change of seasonal precipitation extremes that show a great deal of spatial noise we apply the procedure of spatial smoothing similar to that used in Kharin and Zwiers (2000). The GEV distribution parameters for each grid box are estimated from  $L$ -moments weight-averaged over 9 ( $3 \times 3$ ) adjacent grid boxes. Given the variable model grid, the average is calculated with weights defined by each grid box area. This smoothing procedure implicitly makes assumption that precipitation extremes at a given grid box have statistical characteristics similar to those of extremes at the nearest neighbours. Although the smoothing procedure has certain effect on the regional-scale structure, it allows to estimate the character of the spatial distribution of precipitation extremes.

#### 4. Results

The most disastrous effects of climate extreme events in a region are often related to unusual temperature values or precipitation amounts over different temporal scales. Therefore we estimated the changes in means and extremes (expressed as 30-yr return values) of the

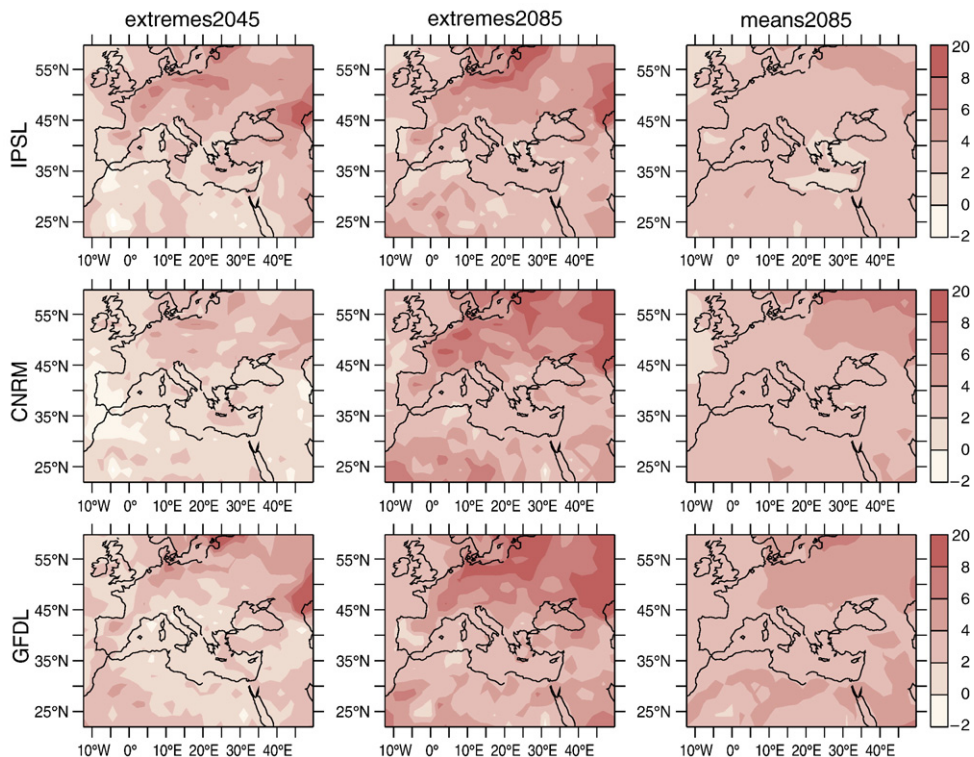


Fig. 5. Future changes of the annual minimum temperature simulated by LMDZ with A2 emission scenario with the three global climate scenarios (IPSL, CNRM and GFDL respectively from top to bottom) relative to 1970/1999: 30-yr return values in 2030/2059 (left panel), 30-yr return values in 2070/2099 (middle panel) and mean values in 2070/2099 (right panel). Units are  $^{\circ}\text{C}$ .

Table 6

Same as in Table 4, but for the annual minimum temperature (°C)

		LMDZ/Control	$\Delta 2045$			$\Delta 2085$		
			LMDZ/IPSL	LMDZ/CNRM	LMDZ/GFDL	LMDZ/IPSL	LMDZ/CNRM	LMDZ/GFDL
NEu	Mean	1.6	1.8	1.2	1.9	2.8	3.1	3.8
	rv30	-12.3	4	2.4	3.1	4.8	5.1	5.8
EEu	Mean	-0.7	2.1	1.1	1.8	3	4	4.1
	rv30	18.4	4.8	2.2	4.2	5.2	6.3	7.3
MEu	Mean	6.7	1.2	0.6	1.5	2.3	2.6	3.2
	rv30	-5.3	2.2	1.2	1.6	2.9	3.5	3.6
NAf	Mean	7.9	1.2	0.8	1.8	2.5	3	3.7
	rv30	-2.9	1.4	0.9	2	3	3.9	3.7
WAs	Mean	3.4	1.9	1	1.9	3.1	3.4	4
	rv30	-11.4	3.1	0.7	1.9	3.4	3.7	4.4

annual minimum temperature, annual maximum temperature and seasonal precipitation in 2039–2059 and in 2070–2099 relative to 1970–1999 for the three global scenarios. We identified the seasons as December–February (DJF), March–May (MAM), June–August (JJA) and September–November (SON). In order to better describe the spatial features of the estimated changes the region was then divided into 5 subregions

named NEu (Northern Europe), EEu (Eastern Europe), MEu (Mediterranean/Europe), NAF (Northern Africa), and WAs (Western Asia) as outlined in Fig. 3. Since we dealt with a variable-grid model we calculated the subregion averages with weights equal to the grid box area divided by the total area of the subregion. Furthermore we estimated changes of the GEV distribution parameters and calculated the spatial correlation

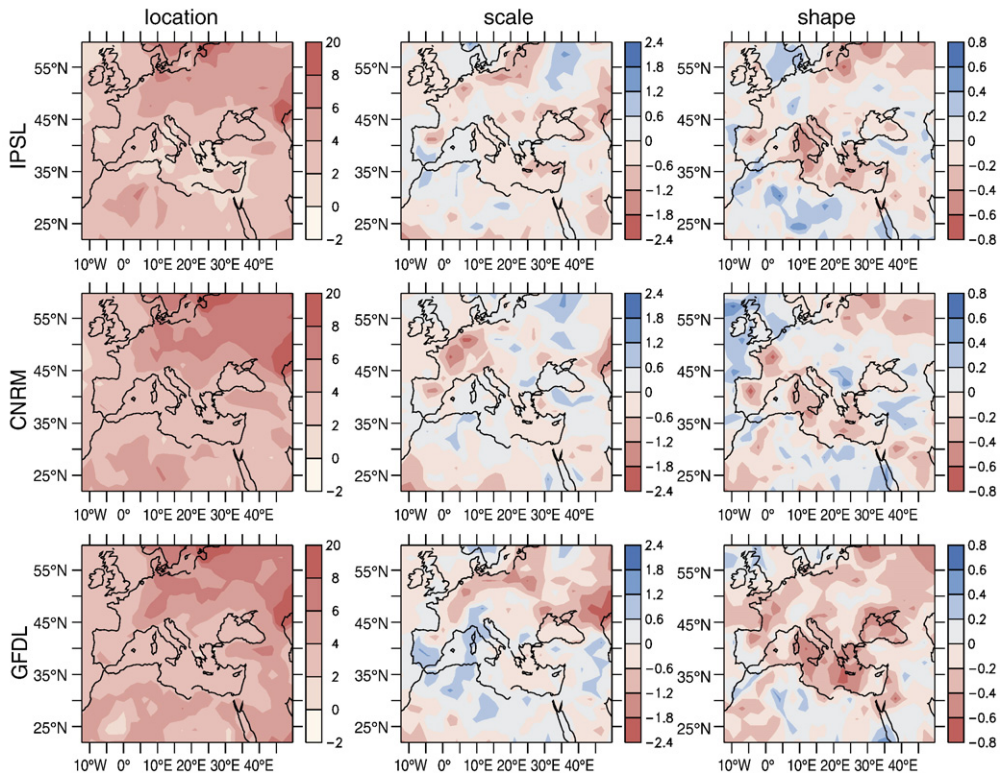


Fig. 6. Changes in location (left panel), scale (middle panel) and shape (right panel) parameters of the GEV distribution of annual minimum temperature simulated by LMDZ with A2 emission scenario with the three global climate scenarios (IPSL, CNRM and GFDL respectively from top to bottom) in 2070/2099 relative to 1970/1999.

Table 7

Same as in Table 5, but for the annual minimum temperature. All the values are statistically significant at the 5% significance level

	$\Delta 2045$			$\Delta 2085$		
	LMDZ/ IPSL	LMDZ/ CNRM	LMDZ/ GFDL	LMDZ/ IPSL	LMDZ/ CNRM	LMDZ/ GFDL
$(\Delta r_{p30}, \Delta \xi)$	0.85	0.67	0.88	0.84	0.9	0.88
$(\Delta r_{p30}, \Delta \alpha)$	-0.82	-0.83	-0.72	-0.61	-0.5	-0.75
$(\Delta r_{p30}, \Delta k)$	-0.28	-0.3	-0.33	-0.25	-0.31	-0.24

between these changes and changes in return values to better understand the nature of variation in extremes.

#### 4.1. Temperature

Changes for the annual maximum temperature are characterized by a high degree of consistency among the three global scenarios, between the middle and the end of the 21st century, as well as between extreme and mean values (Fig. 4, Table 4). Mean annual maximum temperature increases, on average over the region, by 1.5 °C in 2030/2059 and by 3.2 °C in 2070/2099 and has

the greatest magnitudes over southern Europe. Changes in the extremes, expressed as 30-yr return value, are slightly larger (1.6 °C in 2030/2059 and by 3.4 °C in 2070/2099), with a small shift of the maximum to Central Europe.

Three global scenarios produce similar features for the changes in the location parameter (Fig. 4, right column). The scale and shape parameter changes are noisy and have a large dispersion (not shown). Changes in extremes are weakly associated with changes in the location parameter, as shown in Table 5.

Fig. 5 and Table 6 present the annual minimum temperature changes. In general all three global scenarios give similar results revealing increase everywhere with the greatest magnitudes of the warming over Eastern and Northern Europe. Changes are more pronounced in 2070/2099 than in 2030/2059, but have the same spatial features. Changes in extreme agree well with changes in mean but have greater absolute magnitudes (2.4 °C versus 1.5 °C in the middle of the century and 4.5 °C versus 3.3 °C at the end of the century, averaged over the region).

We can see that changes in extremes are only a little larger than changes in means for annual maximum temperature and considerably exceed changes in means

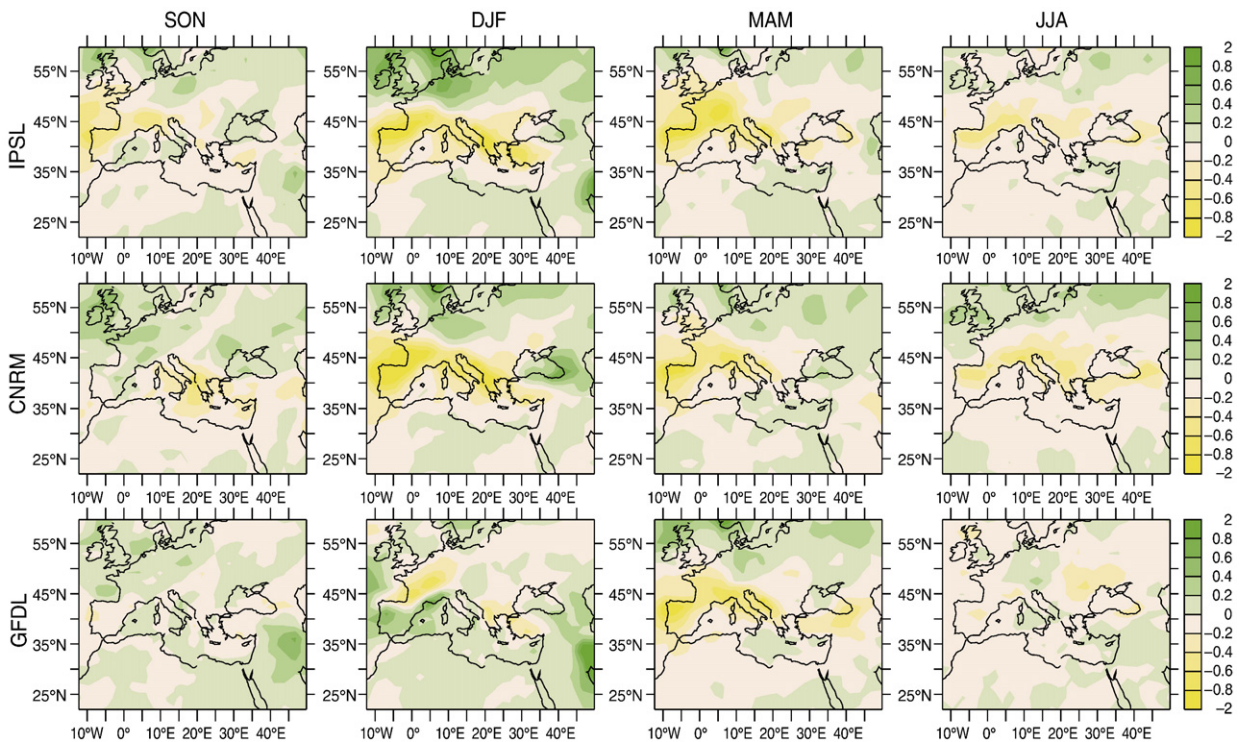


Fig. 7. Future changes in mean precipitation in 2030/2059 relative to 1970/1999 simulated by LMDZ with A2 emission scenario with the three global climate scenarios (IPSL, CNRM and GFDL respectively from top to bottom). Units are mm/day.

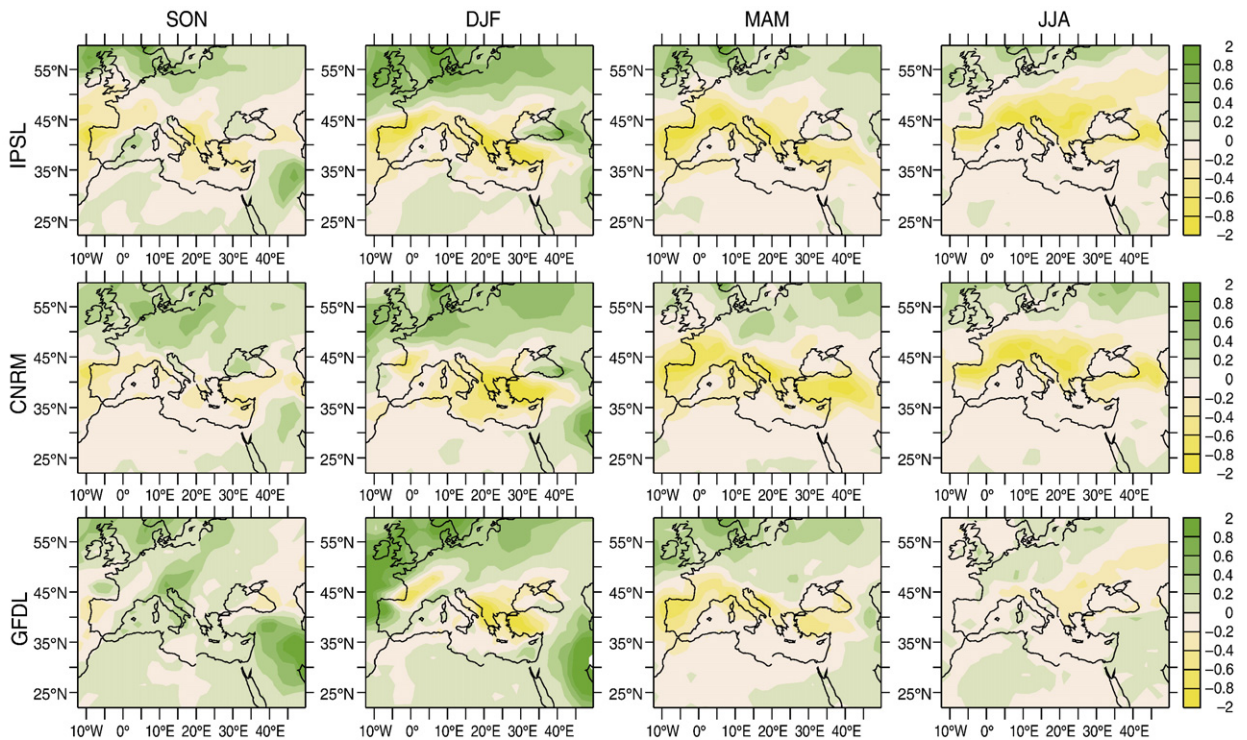


Fig. 8. Same as in Fig. 7, but for 2070/2099 relative to 1970/1999.

for annual minimum temperature. We can further observe that, averaged for the whole domain, changes in means of annual maximum and annual minimum temperature have similar magnitudes (this is true for the absolute values of the changes presented in Tables 4 and 6, as well as for these values expressed as percentage relative to the control climate values). However, the increase in mean maximum temperature is greater than that in mean minimum temperature over the Mediterranean and Southern Europe and the inverse is found

over North and East Europe. Changes in cold extremes exceed respective changes in warm extremes all over the region, except the Mediterranean and Southern Europe.

Fig. 6 shows changes in the location, scale and shape parameters of the GEV distribution for the annual minimum temperature in 2070/2099. Magnitudes and spatial features of changes in location parameter that defines the position of distribution are similar to those of changes in extremes. Changes in the scale and shape parameters are noisier and have greater dispersion

Table 8  
Same as in Table 4 but for winter precipitation (mm/day)

		$\Delta 2045$				$\Delta 2085$		
		LMDZ/Contro	LMDZ/IPSL	LMDZ/CNRM	LMDZ/GFDL	LMDZ/IPSL	LMDZ/CNRM	LMDZ/GFDL
NEu	Mean	3.0	0.4	0.1	-0.0	0.5	0.4	0.5
	rv30	25.8	2.7	2.5	3.4	5.4	3.4	7.4
EEu	Mean	2.0	0.0	0.1	0.0	0.2	0.1	-0.0
	rv30	26.3	1.1	1.6	1.3	3.0	4.2	3.6
MEu	Mean	2.4	-0.3	-0.4	0.0	-0.3	-0.3	-0.1
	rv30	37.0	2.4	0.2	5.2	3.0	3.0	8.2
NAf	Mean	0.1	-0.0	-0.0	0.0	-0.0	-0.0	0.0
WAs	Mean	1.5	0.1	0.1	0.3	0.1	0.1	0.5
	rv30	35.6	5.7	5.7	8.6	9.0	17.7	17.0

Table 9

Same as in Table 4 but for summer precipitation (mm/day)

		$\Delta 2045$				$\Delta 2085$		
		LMDZ/Control	LMDZ/IPSL	LMDZ/CNRM	LMDZ/GFDL	LMDZ/IPSL	LMDZ/CNRM	LMDZ/GFDL
NEu	Mean	1.2	0.0	0.1	-0.1	0.0	0.0	0.0
	rv30	38.4	1.0	3.8	1.7	2.9	4.9	7.9
EEu	Mean	0.7	-0.1	-0.1	-0.1	-0.2	-0.1	-0.1
	rv30	27.8	0.5	-0.5	-0.6	-4.2	-1.9	-0.3
MEu	Mean	0.7	-0.1	-0.2	-0.1	-0.3	-0.3	-0.1
	rv30	26.4	-3.9	0.9	0.2	-0.8	-4.1	-1.1
NAf	Mean	0.0	-0.0	-0.0	-0.0	-0.0	-0.0	-0.0
WAs	Mean	0.3	-0.0	-0.1	-0.0	-0.1	-0.1	0.0

among the three global scenarios. However all the scenarios suggest noticeable decrease of the scale parameter, which is a measure of interannual variability, over the areas where large increase in extremes is found (northwestern coast of Europe and the region north of the Caspian Sea). An increase in mean value of annual minimum temperature and a simultaneous decrease in its interannual variability result in the largest increase of the cold extremes. It is worth to note that this feature is even more pronounced in 2030/2059 (not shown). Previous studies (McGuffie et al., 1999; Meehl et al., 2000; Kharin and Zwiers, 2005) found that the largest changes in minimum temperature occur over world land areas where snow retreats, exposing a lower albedo surface which accelerates in turn warming at the surface. Our results seem to confirm this explanation and suggest further that the greatest decrease of the variability of annual cold extremes takes place in such areas that are snow-covered in some years and snow-free in other years in control climate but almost snow-free in future climate.

Table 7 presents spatial correlation between the changes in extremes of annual minimum temperature and changes in the GEV distribution parameters. Changes in extremes are strongly correlated with changes in

location parameters for the two periods and changes in scale parameter in the middle of the century. There is a moderate correlation between changes in extremes and changes in scale parameter at the end of the century. Correlation between changes in extremes and changes in shape parameter is weak but also statistically significant.

Percentage of grid points where the changes in warm and cold annual extremes are significant at 10% significance level averaged over the three global scenarios is shown in Table 3. The most significant changes are found for the location parameter. The changes in extreme temperature are significant almost everywhere at the end of the century.

#### 4.2. Precipitation

Mean precipitation changes in 2030/2059 and 2070/2099 are presented in Figs. 7 and 8, respectively. The patterns of the changes show a quite good degree of consistency among the three global scenarios within each season, except the intermediate season of autumn. Spatial features of the mean precipitation changes at the end of the century are similar to those in the middle of the century but have greater magnitudes. Mean changes are characterized by a strong reduction belt (up to

Table 10

Same as in Table 4 but for spring precipitation (mm/day)

		$\Delta 2045$				$\Delta 2085$		
		LMDZ/Control	LMDZ/IPSL	LMDZ/CNRM	LMDZ/GFDL	LMDZ/IPSL	LMDZ/CNRM	LMDZ/GFDL
NEu	Mean	2.1	-0.1	0.0	0.1	0.1	0.1	0.2
	rv30	31.1	-0.3	2.0	2.1	3.1	5.6	6.0
EEu	Mean	1.4	-0.1	0.1	-0.0	-0.0	-0.1	-0.1
	rv30	30.2	2.2	1.5	3.2	3.2	2.2	3.6
MEu	Mean	1.6	-0.3	-0.2	-0.3	-0.4	-0.4	-0.3
	rv30	33.2	0.4	1.0	-0.3	0.0	0.5	1.2
NAf	Mean	0.1	-0.0	-0.0	-0.0	-0.0	-0.0	-0.0
WAs	Mean	1.2	-0.0	-0.1	-0.1	-0.1	-0.3	0.0
	rv30	29.8	4.6	5.1	0.6	3.5	2.2	10.8

Table 11

Same as in Table 4 but for autumn precipitation (mm/day)

		$\Delta \bar{2045}$				$\Delta \bar{2085}$		
		LMDZ/Control	LMDZ/IPSL	LMDZ/CNRM	LMDZ/GFDL	LMDZ/IPSL	LMDZ/CNRM	LMDZ/GFDL
NEu	Mean	2.5	0.0	0.1	0.1	0.1	0.3	0.2
	rv30	35.1	0.9	2.8	2.9	3.6	9.1	7.4
EEu	Mean	1.1	0.0	0.1	-0.0	-0.0	0.1	-0.1
	rv30	33.3	1.5	5.1	1.8	4.6	5.2	6.0
MEu	Mean	1.6	-0.1	-0.1	-0.0	-0.2	-0.1	0.1
	rv30	43.5	2.4	1.2	3.3	4.4	5.1	8.6
NAf	Mean	0.1	-0.0	-0.0	0.0	-0.0	-0.0	0.0
	rv30	40.9	7.7	5.7	8.0	8.3	10.1	22.1

-2 mm/day in 2070/2099) over the Mediterranean and South Europe for the DJF, JJA and MAM seasons (Figs. 7, 8, Tables 8–10). There is a small zone of increase over North Europe in summer and a large one for other seasons over the North of our domain and central Europe with the greatest magnitudes (up to 2 mm/day in 2070/2099) in winter.

Spatial patterns of extreme precipitation changes in 2039–2050 are similar to those in 2070/2099 in winter

and autumn, but less pronounced (Tables 8, 11). In spring and summer there is a lower consistency between two future periods (Tables 9, 10) as well as there is no good consistency among the three global scenarios in the middle of the century. This does not necessarily imply discontinuities in evolution of extreme precipitation. This seems to indicate that one needs a longer time period to have a reliable response for precipitation extremes than for mean precipitation or temperature,

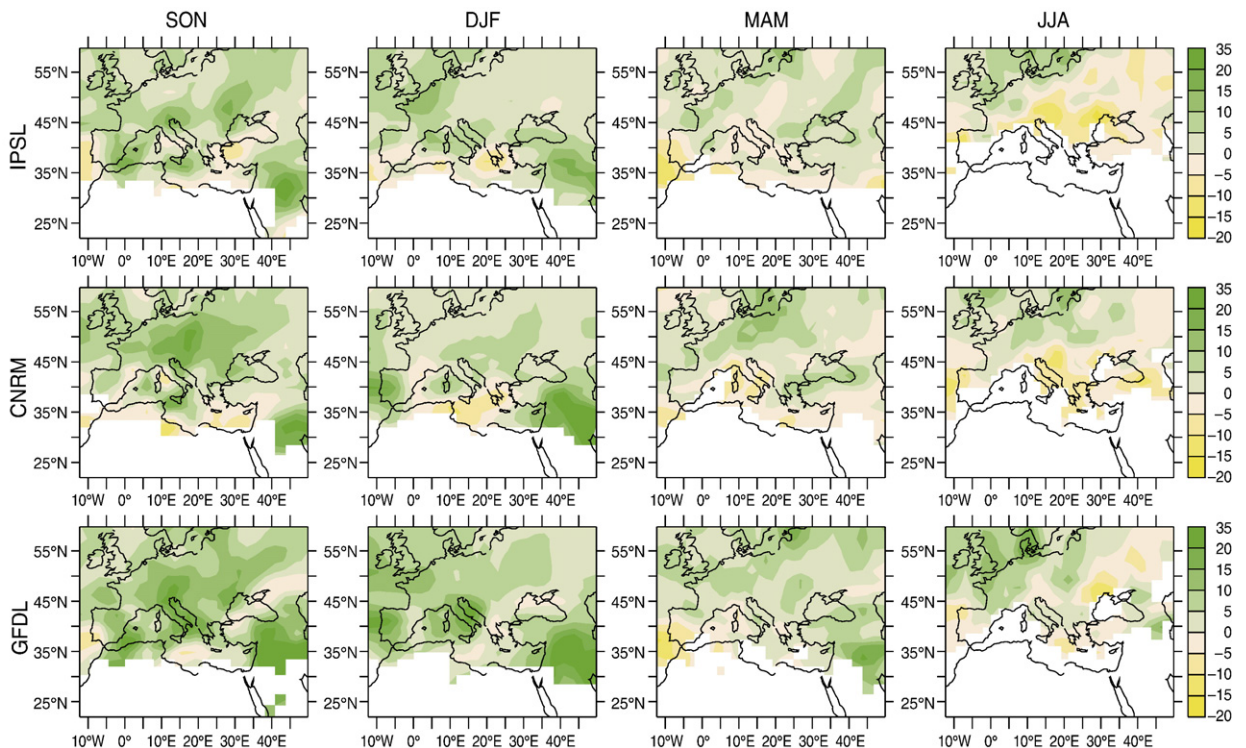


Fig. 9. Future changes of 30-yr return values of extreme precipitation in 2070/2099 relative to 1970/1999 simulated by LMDZ with A2 emission scenario with the three global climate scenarios (IPSL, CNRM and GFDL respectively from top to bottom). Units are mm/day.

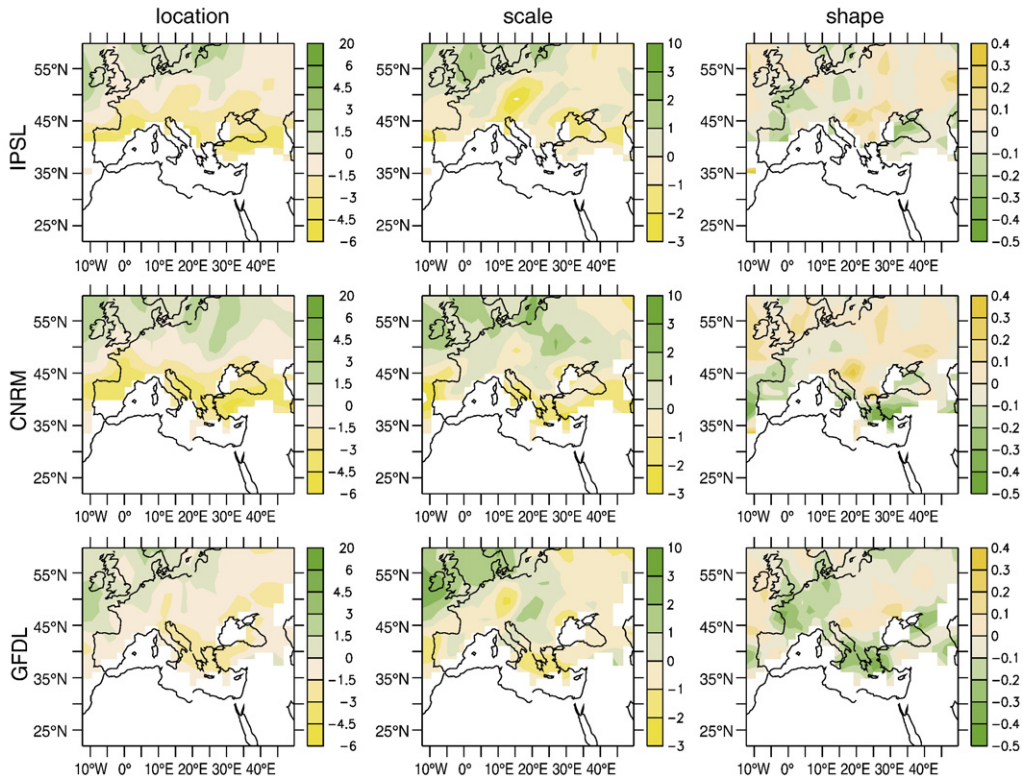


Fig. 10. Changes in location (left panel), scale (middle panel) and shape (right panel) parameters of the GEV distribution of summer precipitation extremes simulated by LMDZ with A2 emission scenario with the three global climate scenarios (IPSL, CNRM and GFDL respectively from top to bottom) in 2070/2099 relative to 1970/1999.

especially for seasons when regional effects and influences are large. Fig. 9 presents changes in 2070/2099, showing main feature similar for three global scenarios. Extremes of precipitation generally increase all over the region in DJF, MAM and SON (Tables 8, 10, 11). The most (in terms of absolute values) considerable changes occur in autumn, the season of most intense precipitation over the region. The winter extreme precipitation is characterized by an important increase over the areas where mean precipitation decreases, except in Greece with decreasing extremes. Increase of intense precipitation in spite of decrease in mean values over the Mediterranean was found by many previous studies (Alpert et al., 2002; Giorgi et al., 2004; Sánchez et al., 2004). These results suggest that precipitation events are rarer in future than at present but characterized by larger daily amounts. Giorgi et al. (2004) and Rodwell et al. (1999) associate the decrease in mean precipitation over southern Europe with a more frequent anticyclonic circulation in this region in future climate. Increasing of heavy precipitation events in the global warming context is suggested to be due to the increased atmospheric

water vapour and warmer air (IPCC, 2001). Meehl et al. (2005) found that in northern Europe the increase of precipitation intensity is also enhanced by advective effects associated with changes in atmospheric circulation.

Figs. 10 and 11 show changes in the parameters of GEV distribution in two seasons (JJA and SON) for intense precipitation in 2070/2099. There is a quite good consistency among the three global scenarios for the location and scale parameters. Shape parameter changes are noisy and have a large dispersion among the global scenarios. In summer (Fig. 10) location parameter decreases everywhere (except Northwest coast of Europe) suggesting decrease of intense precipitation mean values. Scale parameter increases over the Northwest coast of Europe and does not show any regular pattern over the rest of the region. In autumn (Fig. 11) and winter (not shown) location parameter increases over most of the region, except the Mediterranean for the LMDZ/IPSL and LMDZ/CNRM scenarios. In general scale parameters increase considerably all over the region in SON (Fig. 11), DJF and MAM (not shown),

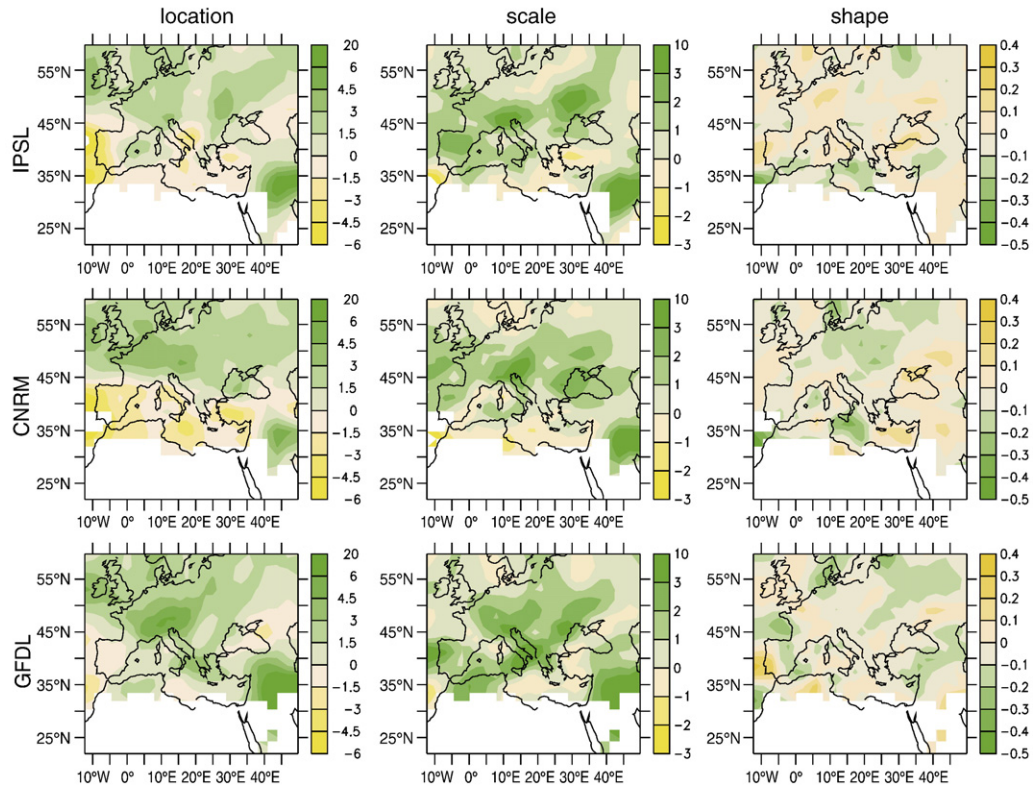


Fig. 11. Same as in Fig. 10 but for the parameters of the distribution of autumn precipitation extremes.

indicating an increase in interannual variability of extreme precipitation.

Table 12 shows that changes in extreme precipitation are weakly correlated with changes in location parameter and moderately correlated with changes in scale and shape parameters for both periods in all the seasons and all the global scenarios.

Changes in 30-yr return values are most significant in winter and summer at the end of 21st century, but even in these cases the percentage of grid points where changes are significant at the 10% significance level does not exceed 50% (Table 3). As for temperature the changes in the location parameter are somewhat more significant.

Table 12

Same as in Table 5, or Table 7, but for precipitation. All the values are statistically significant at the 5% significance level

		$\Delta 2045$			$\Delta 2085$		
		LMDZ/IPSL	LMDZ/CNRM	LMDZ/GFDL	LMDZ/IPSL	LMDZ/CNRM	LMDZ/GFDL
Pre DJF	$(\Delta rp_{30}, \Delta \xi)$	0.31	0.28	0.46	0.34	0.42	0.44
	$(\Delta rp_{30}, \Delta \alpha)$	0.51	0.44	0.56	0.44	0.63	0.66
	$(\Delta rp_{30}, \Delta k)$	-0.49	-0.54	-0.46	-0.55	-0.43	-0.43
Pre JJA	$(\Delta rp_{30}, \Delta \xi)$	0.25	0.35	0.3	0.36	0.35	0.3
	$(\Delta rp_{30}, \Delta \alpha)$	0.5	0.55	0.52	0.58	0.58	0.53
	$(\Delta rp_{30}, \Delta k)$	-0.55	-0.56	-0.59	-0.49	-0.33	-0.52
Pre MAM	$(\Delta rp_{30}, \Delta \xi)$	0.33	0.31	0.36	0.38	0.38	0.41
	$(\Delta rp_{30}, \Delta \alpha)$	0.34	0.42	0.5	0.48	0.54	0.49
	$(\Delta rp_{30}, \Delta k)$	-0.67	-0.62	0.61	-0.55	-0.54	-0.57
Pre SON	$(\Delta rp_{30}, \Delta \xi)$	0.14	0.3	0.14	0.31	0.35	0.44
	$(\Delta rp_{30}, \Delta \alpha)$	0.54	0.56	0.49	0.53	0.55	0.6
	$(\Delta rp_{30}, \Delta k)$	-0.57	-0.59	-0.59	-0.51	-0.51	-0.48

## 5. Summary

In this paper we analyzed potential future changes of the extreme temperature and precipitation around the Mediterranean region for two future periods, 2030/2059 and 2070/2099, respective to the control period 1970/1999 under the A2 emission scenario. The simulations were performed with the variable-grid AGCM LMDZ with zoom over the Mediterranean. The boundary conditions were taken from three different AOGCM (IPSL, CNRM and GFDL) scenarios to estimate uncertainties associated with climate models. Generally speaking, there is a good consistency among the three global scenarios, showing that our results are robust.

Extreme events were described in terms of return values estimated from the GEV distribution of annual or seasonal extremes. We analyzed also changes in the distribution parameters to better understand the nature of the changes in extremes. The following conclusions can be drawn.

1. All the scenarios suggest increase in both annual minimum and annual maximum temperature. For the minimum temperature, the largest warming occurs over Northeast Europe and changes in extremes are a little greater than changes in means. For the maximum temperature, the largest warming is found over South Europe and changes in extremes exceed considerably changes in means. Cold extremes increase more substantially than warm extremes all over the region, except for the Mediterranean and Southern Europe. Changes in temperature extremes are mainly due to the shift of the whole distribution to warmer values. In addition changes in annual cold extremes are also associated with changes in its interannual variability, measured by the scale parameter.
2. Mean precipitations decrease over the Mediterranean and South Europe for the DJF, JJA and MAM seasons. Precipitation extremes, as well as the scale parameter and the interannual variability, generally increase all over the region in DJF, MAM and SON. Changes in precipitation extremes are mostly associated with changes in the scale of the distribution, but also correlated with changes in the location parameter. This result is in agreement with those of [Kharin and Zwiers \(2005\)](#) for global scenarios. Furthermore, we find that precipitation extreme changes are also significantly correlated to changes in shape parameter.
3. For both temperature and precipitation, the response to a global warming is consistent for the two time periods representing the middle and the end of the

21st century. We can thus tentatively conclude that there are no abrupt changes for the Mediterranean region during the 21st century and that the changes at the end of the 21st century are a further amplification of those in the middle of the century.

## Acknowledgement

Computer resources were allocated by the IDRIS, the computer centre of the CNRS. This work is supported by the National French Programme GICC. IPSL data are kindly provided by Jean-Louis Dufresne and Laurent Fairhead. Météo-France data are provided by Michel Déqué, David Salas and Jean-Francois Royer. GFDL data are obtained from: <http://data1.gfdl.noaa.gov/nomads/forms/climate.html>. Comments from two anonymous reviewers are acknowledged to improve the manuscript.

## References

- Alpert, P., Ben-Gei, T., Baharad, A., Benjamini, Y., Yekutieli, D., Colacino, M., Diodato, L., Ramis, C., Homar, V., Romero, R., Michaelides, S., Manes, A., 2002. The paradoxical increase of Mediterranean extreme daily rainfall in spite of decrease in total values. *Geophys. Res. Lett.* 29, 31.1–31.4.
- Babu, G.J., Rao, C.R., 2004. Goodness-of-fit tests when parameters are estimated. *Sankhya, Ser. A* 60 (1), 63–74.
- Christensen, J.H., Carter, T.R., Giorgi, F., 2002. PRUDENCE employs new methods to assess European climate change. *EOS* 83, 147.
- Coles, S., 2001. *An Introduction to Statistical Modeling of Extreme Values*. Springer. 225 pp.
- Delworth, T.L., Stouffer, R.J., Dixon, K.W., Spelman, M.J., Knutson, T.R., Broccoli, A.J., Kushner, P.J., Wetherald, R.T., 2002. Review of simulations of climate variability and change with the GFDL R30 coupled climate model. *Clim. Dyn.* 19 (7), 555–574.
- Dufresne, J.L., Friedlingstein, P., Berthelot, M., Bopp, L., Ciais, P., Fairhead, L., Le Treut, H., Monfray, P., 2002. Effects of climate change due to CO<sub>2</sub> increase on land and ocean carbon uptake. *Geophys. Res. Lett.* 29 (10). doi:10.1029/2001GL013777.
- Durbin, J., 1976. Kolmogorov–Smirnov tests when parameters are estimated. *Lect. Notes Math.* 566, 33–44.
- Emanuel, K.A., 1991. A scheme for representing cumulus convection in large-scale models. *J. Atmos. Sci.* 48, 2313–2335.
- Fisher, R.A., Tippett, L.H.C., 1928. Limiting forms of the frequency distributions of the largest or smallest number of a sample. *Proc. Camb. Philos. Soc.* 24, 180–190.
- Frich, P., Alexander, L.V., Della-Marta, P., Gleason, B., Haylock, M., Klein Tank, A.M.G., Peterson, T., 2002. Observed coherent changes in climatic extremes during the second half of the 20th century. *Clim. Res.* 19, 193–212.
- Gao, X., Pal, J.S., Giorgi, F., 2006. Projected changes in mean and extreme precipitation over the Mediterranean region from a high resolution double nested RCM simulation. *Geophys. Res. Lett.* 33, L03706. doi:10.1029/2005GL024954.
- Gibelin, A.L., Déqué, M., 2003. Anthropogenic climate change over the Mediterranean region simulated by a global variable resolution model. *Clim. Dyn.* 20, 327–339.

- Giorgi, F., Bi, X., Pal, J.S., 2004. Mean, interannual variability and trends in a regional climate change experiment over Europe. II: Climate change scenarios (2071–2100). *Clim. Dyn.* 23, 839–858.
- Hosking, J.R.M., 1990. L-moments: analysis and estimation of distributions using linear combinations of order statistics. *J. R. Stat. Soc., B* 52, 105–124.
- Hosking, J.R.M., 1992. Moments or L-moments? An example comparing the two measures of distributional shape. *Am. Stat.* 46, 186–189.
- IPCC, 2001. *Climate Change 2001: The Scientific Basis, Contribution of Working Group I to the Third Assessment Report of the Intergovernmental Panel on Climate Change*. Cambridge University Press, New York.
- Kharin, V.V., Zwiers, F.W., 2000. Changes in the extremes in an ensemble of transient climate simulations with a coupled atmosphere-ocean GCM. *J. Climate* 13, 3760–3788.
- Kharin, V.V., Zwiers, F.W., 2005. Estimating extremes in transient climate change simulations. *J. Climate* 18, 1156–1173.
- Klein Tank, A.M.G., Können, G.P., 2003. Trends in indices of daily temperature and precipitation extremes in Europe, 1946–99. *J. Climate* 16, 3665–3680.
- Kunkel, K.E., Andsager, K., Easterling, D.R., 1999. Long-term trends in extreme precipitation events over the conterminous United States and Canada. *J. Climate* 12, 2515–2527.
- Li, Z.X., 1999. Ensemble atmospheric GCM simulation of climate interannual variability from 1979 to 1994. *J. Climate* 12, 986–1001.
- McGuffie, K., Henderson-Sellers, A., Holbrook, N., Kothalava, Z., Balachova, O., Hoekstra, J., 1999. Assessing simulations of daily temperature and precipitation variability with global climate models for present and enhanced greenhouse climates. *Int. J. Climatol.* 19, 1–26.
- Meehl, G.A., Zwiers, F.W., Evans, J., Knutson, T., Mearns, L., Whetton, P., 2000. Trends in extreme weather and climate events: issues related to modelling extremes in projections of future climate change. *Bull. Am. Meteor. Soc.* 81, 427–436.
- Meehl, G.A., Arblaster, J.M., Tebaldi, C., 2005. Understanding future patterns of increased precipitation intensity in climate model simulations. *Geophys. Res. Lett.* 32, L18719. doi:10.1029/2005GLO23680.
- Palutikof, J.P., Holt, T., 2004. “Climate change and the occurrence of extremes: some implications for the Mediterranean Basin.” Chapter 4. In: Marquina, A. (Ed.), *Environmental Challenges in the Mediterranean 2000–2050*. Kluwer Academic Publishers, pp. 61–73.
- Rodwell, M.J., Rowell, D.P., Folland, C.K., 1999. Oceanic forcing of the wintertime North Atlantic Oscillation and European climate. *Nature* 398, 320–323.
- Sadourny, R., Laval, K., 1984. January and July performance of the LMD general circulation model. In: Berger, A., Nicolis, C. (Eds.), *New Perspectives in Climate Modelling*. Elsevier, pp. 173–198.
- Sánchez, E., Gallardo, C., Gaertner, M.A., Arribas, A., Castro, M., 2004. Future climate extreme events in the Mediterranean simulated by a regional climate model: a first approach. *Glob. Planet. Change* 44, 73–81.
- Zwiers, F.W., Kharin, V.V., 1998. Changes in the extremes of the climate simulated by CCC GCM2 under CO<sub>2</sub> doubling. *J. Climate* 11, 2200–2222.